A New Index for Remote Sensing of Soil Organic Carbon Based Solely on Visible Wavelengths

Evan A. Thaler*
Isaac J. Larsen
Qian Yu
Dep. of Geosciences
Univ. of Massachusetts
233 Morrill Science Center
Amherst, MA 01003

Remote sensing is a powerful method for mapping soil properties, such as soil organic carbon (SOC), a key property of soil quality. Spectral remote sensing indices that rely on shortwave-infrared (SWIR) or near-infrared (NIR) wavelengths have been developed to quantify spatial patterns in SOC. However, the application of SWIR- and NIR-based indices for quantifying fine-scale patterns of SOC is limited due to the requirement of high-resolution multispectral or hyperspectral imagery. Visible wavelengths are measured by virtually all sensors, often at high resolution; hence, development of a visible wavelength–based index can greatly increase the ability to remotely estimate SOC. Here we develop such an index by assessing the relationship between laboratory-measured SOC and spectral reflectance using 7916 SOC and hyperspectral measurements from the nationwide USDA Rapid Carbon Assessment. Our new SOC index (SOCI) predicts SOC concentrations for the 7916 samples with a RMSE of 1.5%, which is comparable to predictions from the SWIR/NIR ratio (RMSE = 1.3%) and outperforms the predictions of an index based on NIR and red wavelengths (RMSE = 2.8%). We applied the index to a high-resolution satellite image and tested the ability of the image-based SOCI to predict measured SOC concentrations for a plowed field in Iowa. Regression models with and without local calibration data accurately predict measured SOC, with RMSE values of ~0.5%. Given the widespread availability of imagery with spectral data in the visible wavelengths, there is potential to use the SOCI to address a range of soil-agronomic problems.

Abbreviations: DN, digital number; NIR, near-infrared; RaCA, USDA Rapid Carbon Assessment; SI, spectral index; SOC, soil organic carbon; SOCI, soil organic carbon index; SWIR, shortwave-infrared; VIS, visible; ρ, spectral reflectance.

Core Ideas

- **A soil carbon remote sensing index was developed using visible wavelengths.**
- **The new index performs as well as or better than existing indices.**
- **The new index can be applied to any true color image to map soil organic carbon.**

Soil organic carbon (SOC) is vital for soil fertility and agricultural productivity (Lal, 2006; Reeves, 1997). Soil erosion causes declines in SOC, which result in economic losses due to decreased crop productivity (Lal, 2004; West and Post, 2002) and the need to supplement degraded soils with chemical fertilizers (Pimentel et al., 1995). The influence of SOC on agricultural productivity has, in part, driven interest in the development of digital soil mapping techniques (Bachofer et al., 2015; Chen et al., 2000; Dogan and Kılıç, 2013; Frazier and Cheng, 1989; Mishra et al., 2009; Mulder et al., 2011). Digital soil mapping techniques use diffuse reflectance spectroscopy, which has been demonstrated to accurately and nondestructively relate spectral reflectance to soil properties (Bachofer et al., 2015; Ben-Dor and Banin, 1995; Gomez et al., 2008; Peón et al., 2017). Digital soil mapping has been used to qualitatively assess the degree of soil degradation in agricultural landscapes by categorizing the degradation into severity classes (Chikhaoui et al., 2005) and to quantitatively predict SOC concentrations (Chen et al., 2000; Gomez et al., 2008; Frazier and Cheng, 1989; Rossel et al., 2006). The use of spectrographic analysis to digitally map soil characteristics has been used in precision agriculture because rapid, field-scale assessments of soil properties allow farmers to efficiently identify and treat soils in which nutrients are limited (Mulla, 2013).

Soil Sci. Soc. Am. J. 83:1443–1450
doi:10.2136/sssaj2018.09.0318
Received 3 Sep. 2018.
Accepted 15 May 2019.
*Corresponding author (ethaler@geo.umass.edu).

Linear regression models developed from laboratory hyperspectral reflectance and chemical measurements of soil samples have often been used to calibrate spectral indices for predicting soil properties based on soil color (Bachofer et al., 2015; Ben-Dor and Banin, 1995; Frazier and Cheng, 1989; Gomez et al., 2008; Mulder et al., 2011; Nanni and Demattê, 2006). Soil color often varies due to changes in SOC and soil moisture (Escadafal, 1993; Schulze et al., 1993). Soils with higher SOC concentrations are typically darker colored and therefore have lower spectral reflectance than soils with lower SOC content (Rossel et al., 2006). Similarly, increasing soil moisture causes soils to appear darker because the reflectance of incident radiation in the visible spectrum uniformly decreases with increasing moisture (Nocita et al., 2013; Weidong et al., 2002). However, unlike reflectance changes due to SOC content, the uniform decrease in reflectance across the visible wavelengths with increasing soil moisture indicates that use of band ratios can remove the impact of soil moisture on spectral reflectance (Nocita et al., 2013; Stoner and Baumgardner, 1981).

Wavelengths in the short-wave infrared (SWIR, 1300–2500 nm) and near-infrared (NIR, 700–1300 nm) regions have been shown to be sensitive to SOC, with the reflectance in both regions decreasing with increasing SOC (Bartholomeus et al., 2008). Several spectral indices that are sensitive to changes in SOC have been derived using laboratory and field measurements of SWIR and NIR reflectance, ρ (Peón et al., 2017; Rossel et al., 2006). For example, the band ratio SWIR/NIR (ρ_{1608}/ρ_{833} nm) was correlated with SOC ($R^2 = 0.98$) for 32 soil samples and used to examine the extent of SOC-rich topsoil erosion in the Palouse region of eastern Washington (Frazier and Cheng, 1989). For most satellite sensors, measurements of wavelengths in the SWIR region are limited in pixel resolution or, where SWIR is measured at high pixel resolution, in the coverage and availability of images. Hence, there are limitations to implementing SWIR-based indices at fine-spatial scales. Because visible wavelengths are measured by most sensors and can rapidly be measured at the field scale using satellites, unmanned aerial vehicles (drones), or other platforms, the development of an SOC index based solely on the visible spectrum would allow variations in SOC to be efficiently assessed without the use of multispectral or hyperspectral imagery that include data in the SWIR-NIR wavelengths.

Spectral methods that use combinations of visible (VIS, 400–700 nm) and NIR bands (Chen et al., 2000; Peón et al., 2017) have been developed for small geographical areas but have not been calibrated using data from larger spatial scales. For example, image intensity values in the VIS wavelengths calculated from an aerial image of a 115-ha field in Georgia were used to develop a multiple linear regression model that predicted SOC with an R^2 of 0.93; however, the regression was calibrated using only 28 soil samples (Chen et al., 2000). A spectral index (SI) with the form of the normalized difference vegetation index [$SI_{1001–679\ nm} = (\rho_{1001} - \rho_{679})/(\rho_{1001} + \rho_{679})$], which is typically used in phenological studies of vegetation, has been shown to be useful as an SOC index (Peón et al., 2017). A maximum R^2 value of 0.56 was observed for the correlation between SOC and the $SI_{1001–679\ nm}$ calculated from satellite hyperspectral measurements from 39 soil samples collected in northwestern Spain (Peón et al., 2017). Although SOC has been shown to be well correlated with the SWIR/NIR and $SI_{1001–679\ nm}$ indices, such studies have used a relatively small number of soil samples collected from a limited geographic extent. Hence, the utility of such indices at regional to global scales remains untested.

In addition to using diffuse reflectance spectroscopy to develop spectral indices, the application of multivariate statistical techniques or machine learning algorithms, such as principal component analysis (Chang et al., 2001), regression trees (Peón et al., 2017), support vector machines (Aldana-Jague et al., 2016), artificial neural networks (Rossel and Behrens, 2010), and partial least squares regression (Rossel et al., 2006), are used for SOC estimation. For example, artificial neural networks were used with hyperspectral data from ~20,000 soil samples collected by the USDA Rapid Carbon Assessment (RaCA) to develop models for predicting SOC (Soil Survey Staff, 2013). Incorporating land use, master horizon, and textural class information into the models resulted in SOC predictions with RMSE values between 0.5 and 1.5% (Wijewardane et al., 2016). However, transferring such multivariate statistical models between sensors is complex because wavelength position, bandwidth, and number of bands vary between sensors (Li et al., 2012). Multivariate and machine learning techniques are hence specific to the sensors for which they are derived and require re-calibration for use with different sensors (Bartholomeus et al., 2008).

Although multiple approaches have been used to predict SOC from spectral data, there remains a need for the development of a spectral index for SOC, based on wavelengths in the visible range, that can be applied to multispectral and hyperspectral imagery at high spatial resolution (Peón et al., 2017). Here we use SOC measurements and hyperspectral reflectance data for soil samples collected across the United States to compare a newly developed index that relies only on the VIS wavelengths to the SWIR/NIR and the $SI_{1001–679\ nm}$ indices. We then validate the new index using a satellite image to generate a map of predicted SOC values for a field in Iowa and compare the predictions against measured SOC concentrations.

DATA AND METHODS

Laboratory data

The RaCA, undertaken by the Soil Science Division of the USDA National Resource Conservation Service, collected 144,833 soil samples to 1 m depth at 6148 sites in the conterminous United States (Soil Survey Staff, 2013; Wills et al., 2014). Soil samples were air-dried and sieved to <2 mm, and hyperspectral reflectance was measured from 350 to 2500 nm for all samples using an ASD Labspec Spectrometer (Analytical Spectral Devices, Inc., PANalytical NIR Excellent Center). The SOC concentration was measured for a subset of samples as the difference between total C and inorganic C (Wijewardane et al., 2016). To evaluate the ability of existing SOC indices and a new index based solely on the visible spectrum to predict SOC, we used 7916 measurements of SOC and hyperspectral reflectance from the RaCA for mineral soil horizons (A- and B- horizons) from 2673 locations within the conterminous United States (Fig. 1).

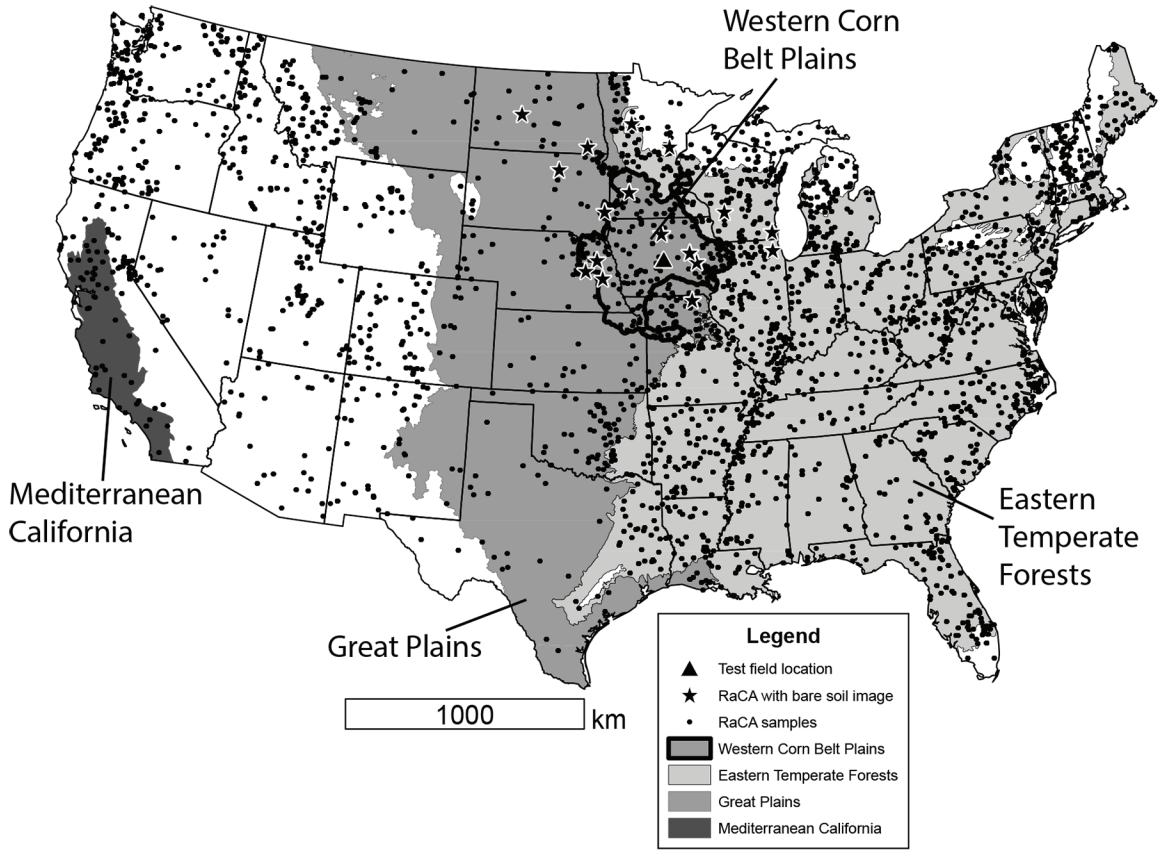

Fig. 1. Map of USDA Rapid Carbon Assessment (RaCA) soil sample locations and USEPA ecoregions: The Great Plains, Mediterranean California, and Eastern Forests Level I ecoregions and the Level III Western Corn Belt Plains region. The RaCA sample locations are shown as black circles. Black stars are locations of calibration sites where RaCA samples were collected; bare soil is exposed in a WorldView-2 (DigitalGlobe, https://www.digitalglobe.com) satellite image. The field where 228 soil samples were measured for soil organic C (Li et al., 2018) is marked as a black triangle.

Development of a New Spectral Index and Comparison with Existing Indices

We developed a new SOC index (SOCI) by performing linear regression between combinations of visible bands and SOC using the national RaCA soil sample data and choosing a combination of bands that minimized the RMSE (Supplemental Table S1). We term the band combination that yielded the minimum RMSE value the SOCI:

$$SOCI=\frac{\rho_{Blue}}{\rho_{Red}\cdot\rho_{Green}} \quad [1]$$

We used reflectance at 478, 546, and 659 nm for blue, green, and red, respectively, which correspond to the center wavelengths of the WorldView-2 sensor.

Soil properties, such as SOC concentrations, exhibit high degrees of spatial correlation (Cambardella et al., 1994; Mishra et al., 2009); hence, the strength of relationships between remote sensing indices and measured SOC values likely varies with spatial scale between and within regions due to differences in predominant soil forming factors. To assess the role of scale and regional variability, we examined the R^2 and RMSE between measured SOC and the SOCI, the SWIR/NIR index, and the $SI_{1001–679\ nm}$ for RaCA soil sample datasets of varying spatial extent: the conterminous United States, three large and predominantly agricultural USEPA Level I ecoregions (Great Plains, Eastern Temperate Forests, and Mediterranean California), and 54 Level III ecoregions nested within the larger Level I ecoregions (Omernik, 1987).

Application of the New Index to Soil Organic C Mapping Using Satellite Imagery

We used a 1.9-m pixel resolution WorldView-2 satellite image of a 15-ha agricultural field in Iowa to assess the ability of the SOCI to predict spatial patterns in SOC. Within the field, previous workers collected 228 soil samples to a depth of 30 cm (Li et al., 2018). The samples were sieved to <2 mm and ground to a powder, and the depth-averaged SOC concentrations for the 30-cm profile were measured (Li et al., 2018). The image was acquired on 4 May 2010, when the field was plowed and lacked both crop residue and crop cover. We used the SOCI to predict SOC within the field using two methods: (i) we used a subset of the measurements from the field to locally calibrate a relationship between the SOCI and SOC and then used the local calibration to predict measured SOC values, and (ii) we developed a regional calibration between the SOCI and SOC using RaCA data from the Western Corn Belt Plains Level III ecoregion, where the agricultural field is located, and used the regional calibration to predict SOC.

Local Calibration

To determine if radiometric correction of the image is necessary for the index to be applied, we calculated the SOCI from

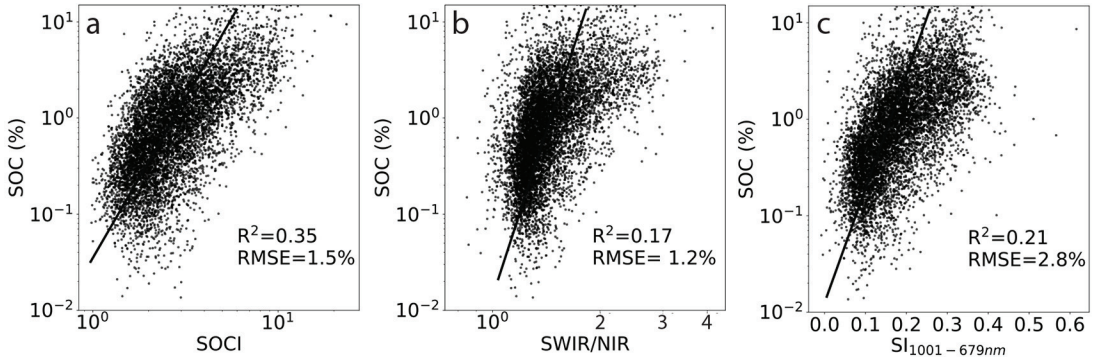

Fig. 2. Spectral indices versus soil organic C (SOC) for the nationwide dataset (n = 7916) for (a) the soil organic C index (SOCI) developed in this study, (b) the shortwave-infrared (SWIR)/ near-infrared (NIR) index, and (c) the spectral index (SI)1001–679 nm. Black lines show the regression for each index.

the uncorrected, raw 11-bit digital number (DN) image and from reflectance data derived by radiometrically calibrating the image. The image was radiometrically corrected to derive reflectance using an empirical line calibration method (Smith and Milton, 1999). A deep, clear water pixel and an aluminum metal roof pixel were identified and calibrated against reflectance values for distilled water and aluminum metal roofing from the ASTER spectral library (Baldridge et al., 2009). The SOCI was then calculated from the reflectance data. For the DN image and the reflectance image, we extracted the SOCI from each pixel with a corresponding soil sample. We predicted SOC for each sample location by developing a linear regression between SOC and the SOCI using a calibration dataset of 45 random samples (20%) of the measured SOC concentrations and SOCI values from both the DN and reflectance images. We then used the calibration to predict SOC for the remaining 183 pixels where samples were collected.

Regional Calibration

The RaCA calibration data are based on laboratory spectral measurements rather than on satellite-based measurements. Hence, we first needed to account for offset between the satellite- and laboratory-derived indices, which arise due to different measurement conditions, such as sieving of laboratory samples and imperfect radiometric correction. We scaled the satellite-derived index to the laboratory-derived index by developing a linear regression relationship between satellite- and laboratory-derived SOCI using reflectance data from 16 locations where an RaCA sample was collected from a location with a WorldView-2 satellite image with bare soil at the sample site.

The SOCI data derived from imagery predict SOC concentrations for the soil surface, but the measured SOC values are an average concentration for a depth interval extending from the soil surface to a depth of 30 cm (Li et al., 2018). To compare the SOC predictions from the satellite-derived SOCI values with the measured SOC values, we scaled the predicted SOC values to an average SOC concentration for the upper 30 cm of the soil profile by assuming an exponential depth-distribution of SOC (Mishra et al., 2009):

$$\text{SOC} = ae^{bz} \qquad [2]$$

where a and b are fitted parameters describing the surface SOC concentration and the rate of decay, respectively, and z is depth within the profile. The depth at which the average SOC concentration occurs is described by $1/b$ (Lilliefors, 1969). The a and b parameters are not available for the field in Iowa, so we determined them by fitting Eq. [2] to 15 SOC-depth profiles with five or more SOC-depth measurements at RaCA sites in the Western Corn Belt Plains Level III ecoregion. We used the average of the a and b parameters from all profiles to calculate the average SOC for the upper 30 cm of the soil. The surface- and depth-averaged predictions were compared against the depth-averaged measurements. All statistical analyses were performed using the NumPy (version 1.14.3) and SciPy (version 0.18.1) packages in Python 3.

RESULTS

Index Validation Using Laboratory Spectral Data

For the nationwide dataset of SOC measurements, the SOCI, SWIR/NIR, and $SI_{1001–679\ nm}$ indices are similarly correlated with SOC. The SOCI has a power-law relationship with SOC (Fig. 2a) and has an R^2 of 0.35 and RMSE of 1.5%. The SWIR/NIR index also has a power-law relationship with SOC (Fig. 2b), where the R^2 is 0.17 and the RMSE is 1.2%. The $SI_{1001–679\ nm}$ is exponentially correlated with SOC (Fig. 2c), where the R^2 is 0.21 and the RMSE is 2.8%. (Table 1)

Results from the Level I ecoregions indicate there were higher correlation coefficients and lower errors for the Great Plains and Mediterranean ecoregions relative to the nationwide data (Table 1). The respective Great Plains and Mediterranean California Level I ecoregion RMSE values for the SOCI were 1.4 and 1.8%, which were comparable to the SWIR/NIR index values of 0.98 and 1.3%, both of which were lower than the $SI_{1001–679\ nm}$ values of 3.3 and 4.1%. Results from the Eastern Temperate Forests Level I ecoregion were comparable to values from the nationwide analysis; RMSE values were similar for the SOCI (1.5%) and were slightly higher for the SWIR/NIR index (1.3%) and the value for the $SI_{1001–679\ nm}$ index was higher (4.1%). Generally, the results for the 54 Level III ecoregions had lower errors and higher correlations than the Level I ecoregions (Supplemental Table S2). The RMSE values for SOCI (0.42–2.6%) were comparable to the SWIR/

Table 1. Equations, correlation coefficients, and RMSE values for soil organic carbon (SOC) prediction using the three spectral indices for the national dataset, three major US agricultural Level I ecoregions, and the Western Corn Belt Level III ecoregion.

				Level I ecoregions						Level III ecoregion‡	
		Nationwide (n = 7916)		Great Plains (n = 1767)		Eastern Forests (n = 4243)		Mediterranean California (n = 153)		Western Corn Belt Plains (n = 595)	
Spectral index†	**Relationship with SOC using national data**	R^2	RMSE	R^2	RMSE	R^2	RMSE	R^2	RMSE	R^2	RMSE
SOCI	$SOC = 0.3 \cdot SOCI^{1.4}$	0.35	1.5%	0.43	1.4%	0.31	1.5%	0.36	1.8%	0.54	1.0%
SWIR/NIR	$SOC = 0.7 \cdot SWIR/NIR^{2.2}$	0.17	1.2%	0.36	0.98%	0.13	1.3%	0.26	1.3%	0.46	1.4%
$SI_{1001-679\ nm}$	$SOC = 1.6 \cdot e^{3.7 \cdot SI1001-679\ nm} - 1.7$	0.21	2.8%	0.29	3.3%	0.18	4.1%	0.31	2.9%	0.42	2.7%

† NIR, near-infrared; SOCI, soil organic carbon index; SWIR/NIR, shortwave-infrared and near-infrared; SI, spectral index.

‡ Data from all 54 Level III ecoregions are shown in Supplemental Table S2.

NIR values (0.43–1.9%), and both were lower than those from the $SI_{1001-679\ nm}$ (0.60–9.1%) (Fig. 3; Supplemental Table S2).

Index Validation Using Satellite Image

Local Calibration

The calibration dataset derived from the SOC measurements in the field (Fig. 4a) and the SOCI calculated from the DN image (Fig. 4b) predicted SOC with a RMSE of 0.53% (Fig. 4c). Similarly, when the SOCI was calculated from the reflectance image, the local calibration (Fig. 4d) predicted SOC with a RMSE of 0.54% (Fig. 4e).

Regional Calibration

The comparison of SOCI values calculated from colocated RaCA soil samples and WorldView-2 imagery indicates the two indices are linearly correlated (R^2 = 0.82) (Fig. 5). Because the SOCI values are well correlated, the regression relationship was used to scale WorldView-2 satellite–derived SOCI values to the same range of SOCI values determined from the RaCA samples. The scaled, regionally calibrated SOCI, based on the RaCA samples, generated SOC predictions that were comparable to the calibrations that were locally calibrated, but only after accounting for depth-averaged SOC concentrations. We found that surface SOC concentrations predicted from the satellite image are correlated to the average SOC for the upper 30 cm of the soil profile (R^2 = 0.66; RMSE = 4.8% SOC) (Fig. 6a). However, after estimating the average SOC concentration within the upper 30 cm of the profile using an exponential decay function (Fig. 6b), the RMSE improved to 0.54% SOC (Fig. 6c).

DISCUSSION

The SOCI is effective at estimating SOC because it tracks changes in the reflectance of the red and green wavelengths, which have been demonstrated to be relevant for SOC estimations (Bartholomeus et al., 2008; Stevens et al., 2010). The slopes of reflectance curves in the visible wavelengths generally decline as a function of SOC, and the reflectance values for each of the visible wavelengths decrease with increasing SOC (Fig. 7). Concentrations of pedogenic iron-bearing minerals, which impart a red hue to soil, have been found to be inversely correlated to concentrations of SOC, such that soils with a red hue often have less organic matter and more iron oxide minerals than dark-colored, SOC-rich soils (Frazier and Cheng, 1989; Palacios-Orueta and Ustin, 1998). Hence, soils enriched in pedogenic iron relative to SOC have increased reflectance in the red and green wavelengths relative to soils enriched in SOC (Huete and Escadafal, 1991; Palacios-Orueta and Ustin, 1998). The large increase in red and green reflectance in samples with low SOC, relative to darker samples with high SOC (Fig. 6), results in decreased SOCI values.

For the national dataset, the three Level I ecoregions, and the 54 Level III ecoregions, the ability of the SOCI to predict SOC is comparable to the predictive power of the SWIR/NIR index and better than the $SI_{1001-679\ nm}$ index. An artificial neural network model, developed using ~20,000 samples from the RaCA database that incorporated textural as well as spectral information about the soil samples, predicted SOC, with RMSE values that ranged from 0.5 to 1.5% (Wijewardane et al., 2016). Likewise, using a dataset of ~8600 samples from the RaCA, a random forest model, which also included horizon and texture information, was able to predict SOC, with RMSE values ranging from 2.0 to 2.5% (Sequeira et al., 2014). The SOCI performance for the national and Level I ecoregion datasets (RMSE 1.5–1.8%) is within the range of or slightly better than these multivariate techniques, which, along with its similar performance to the SWIR/NIR index, indicates that the SOCI has potential for SOC prediction. Furthermore, because the SOCI uses fewer wavelengths for predictions than multivariate and machine learning methods, it can be readily applied to multispectral imagery, as demonstrated by the calculation of the index from the WorldView-2 data (Fig. 5 and 6).

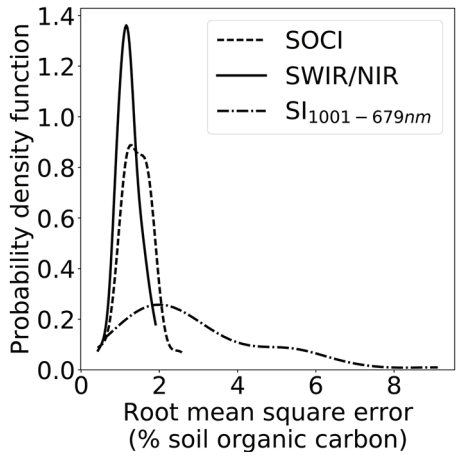

Fig. 3. Probability density function of RMSE values for the three indices calculated for each of the 54 Level III ecoregions. NIR, near-infrared; SI, spectral index; SWIR, shortwave-infrared.

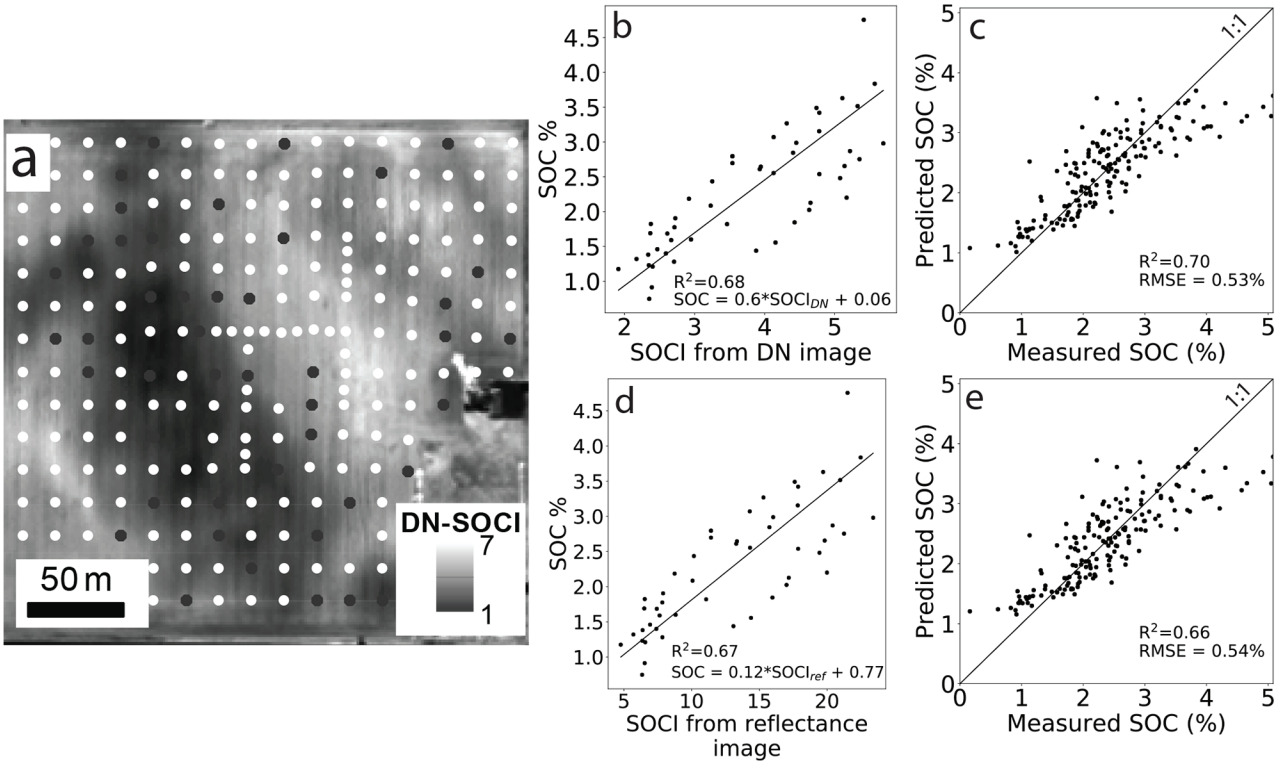

Fig. 4. (a) Map of the soil organic C (SOC) index (SOCI) calculated from a digital number (DN) image of a field in Iowa where SOC was measured in 228 soil samples (Li et al., 2018). Sample locations are shown as circles; those shown in black are the random 20% selection used in the calibration. (b) Measured SOC versus SOCI values derived from the DN image (R^2 = 0.68). (c) Predicted SOC versus measured SOC, where predictions are calculated from the relationship shown in (b). The predicted SOC is correlated with measured SOC with R^2 = 0.70 and RMSE = 0.53%. (d) Measured SOC versus SOCI values derived from the reflectance image for the calibration dataset (R^2 = 0.67). (e) Predicted SOC vs. measured SOC, where predictions are calculated from the relationship shown in (d). The predicted SOC is correlated with measured SOC, with R^2 = 0.66 and RMSE = 0.54%.

The application of the SOCI to the WorldView-2 image of the field in Iowa, where soil properties are less variable than in the nationwide and ecoregion datasets, provides a test of its ability to predict SOC. There, SOCI is well correlated with SOC (RMSE = ~0.5%), demonstrating that the index is a useful method for remotely measuring SOC. Because the SOCI relies only on the visible spectrum, it has potential to be more widely applied than the SWIR/NIR index because SWIR and NIR wavelengths are often not available or are much costlier for very-high-resolution satellite sensors (≤4 m). For example, the SOC predictions for the field in Iowa would not be possible with the SWIR/NIR index, given the current resolution and library of SWIR imagery. Due to spatial variability in factors such as topography and erosion, SOC varies widely on small spatial scales; for example, within the 15-ha field in Iowa, SOC ranges from 0.2 to 5.0% (Li et al., 2018). Publicly available platforms with global coverage of SWIR measurements (e.g., Landsat OLI, ASTER) often measure SWIR at 30 m spatial resolution (Roy et al., 2014). Such coarse-resolution pixels are a mixture of soil properties (Adams et al., 1986), limiting the spatial scale at which SWIR-based indices can be used to predict SOC concentrations. Although there are satellite sensors that measure in the SWIR region at high spatial resolution, the library of images is not yet as spatially extensive as VIS data from other platforms.

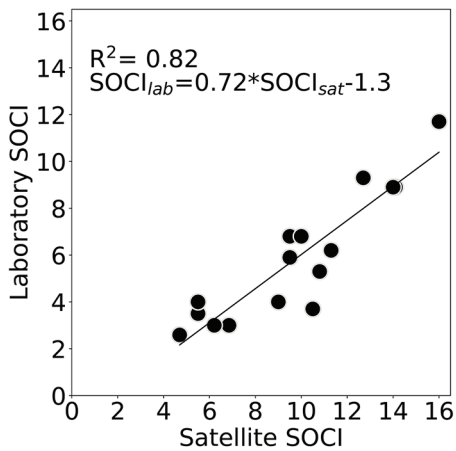

Fig. 5. The soil organic C index (SOCI) derived from USDA Rapid Carbon Assessment laboratory spectral data versus SOCI derived from WorldView-2 satellite imagery spectral data (n = 16).

Application of SOCI to imagery of plowed agricultural fields with exposed soil has the potential to provide a rapid and robust qualitative assessment of the distribution of degraded soils from field to regional scales as well as quantitative estimates of SOC. The SOCI can be applied to SOC prediction in at least two ways. For example, within the RaCA study region, the SOCI can be calculated from radiometrically calibrated imagery and scaled to the RaCA-derived values (Fig. 4d). Soil organic C can then be predicted using the regression relationships that are listed in Supplemental Table S2 between SOC and SOCI for the ecoregion of interest. For areas where data like those in the RaCA database do not exist, regression relationships be-

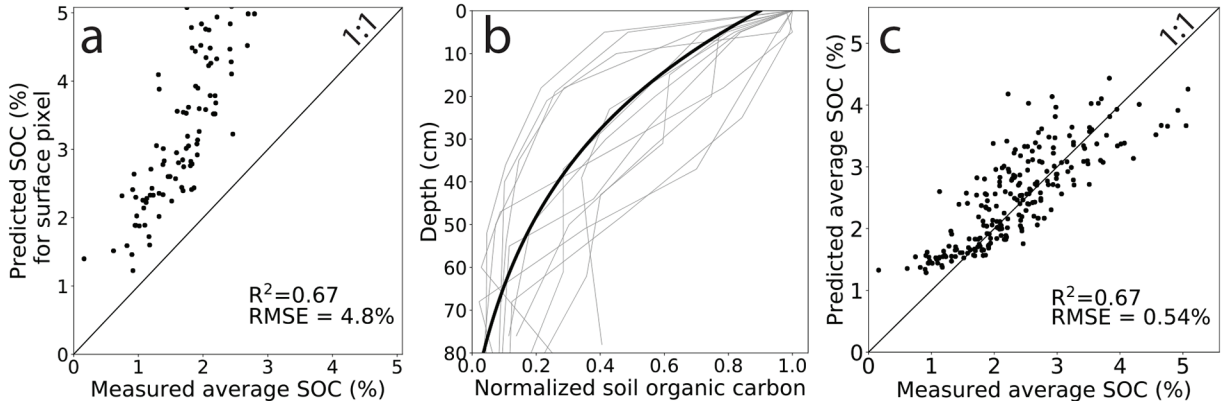

Fig. 6. (a) Soil organic C (SOC) predicted for a surface pixel versus the measured average SOC for a 30-cm profile (R^2 = 0.67; RMSE = 4.8%). (b) The SOC-depth curves for 15 USDA Rapid Carbon Assessment sites within the Western Corn Belt Plains ecoregion (gray lines) and the average exponential function (black line), where *a* and *b* from Eq. [2] are 3.5% SOC −13.1, respectively. The SOC-depth profiles are normalized by the maximum SOC concentration for each profile. (c) Same data as in (a), except the predicted values have been scaled to the mean values for the upper 30 cm of the soil using the average exponential function in (b). The predicted SOC is linearly correlated to the measured SOC with R^2 = 0.67 and an RMSE of 0.54% SOC.

tween SOC and the SOCI can be locally developed from laboratory and satellite spectral data and SOC measurements to predict SOC. Alternatively, the strong correlation between SOC and the SOCI calculated from the DN image (Fig. 4c), as well as the similarity in the RMSE between the DN- and reflectance-derived SOCI values, suggests that raw imagery can be used to estimate the concentration of SOC without performing radiometric correction. Such a finding implies that any true-color image can be used to estimate SOC, including those collected from cameras on manned or unmanned aerial vehicles. The SOCI hence provides the ability to rapidly perform large-scale, high-resolution assessments of C stocks and to identify SOC-poor soils within agricultural fields. Such information can guide agriculture land management decisions by allowing farmers to target SOC-depleted soils for remediation and precision nutrient application (McCarty and Reeves, 2006; Rossel et al., 2006).

CONCLUSIONS

We used 7916 hyperspectral and SOC measurements from soil samples collected by the USDA Rapid Carbon Assessment from the conterminous United States to develop a new spectral index for predicting SOC concentrations that uses only the visible (red, green, and blue) wavelengths. We find that our new index performs similarly to the SWIR/NIR index and better than the $SI_{1001–679\ nm}$ index, both of which rely on longer wavelengths than those in the visible spectrum. We calculated the new index on a high-resolution WorldView-2 image of a field in Iowa where SOC had previously been measured to test its ability to predict SOC concentrations. With local calibration data, the new SOCI calculated from both a raw image and a radiometrically corrected reflectance image predicts SOC concentrations with an RMSE of ~0.5%, indicating that, with the use of local calibration data, radiometric correction of imagery is not necessary for application of the index. We also showed that the SOCI can be used to predict SOC with a region-wide calibration by scaling the WorldView-2 satellite spectra to the same range as the Rapid Carbon Assessment laboratory spectra, where the index predicted measured SOC values with a RMSE of 0.54%. Because the new index relies only on the visible spectrum, it can be used to predict SOC using any true color image, which are captured by most satellite sensors and cameras, including those mounted on unmanned aerial vehicles, at increasingly high spatial resolution. Hence, the index has the potential to be widely applied to map SOC at the field to regional scale. Such maps have a wide range of potential applications for informing C budgets and guiding soil management.

ACKNOWLEDGMENTS

The research was funded by NASA grant 80NSSCK0747 (to I. Larsen). We thank Skye Wills and the USDA–NRCS National Soil Survey Center for access to the laboratory data from the Rapid Carbon Assessment, Elizabeth Hoy of NASA for assistance accessing imagery, and Xia Li for sharing published soil organic carbon data and an anonymous reviewer.

SUPPLEMENTARY MATERIAL

The supplementary material includes a table of the combinations of visible band wavelengths used to develop the index and a table of equations, correlation coefficients, and RMSE of each index for all 54 Level III ecoregions.

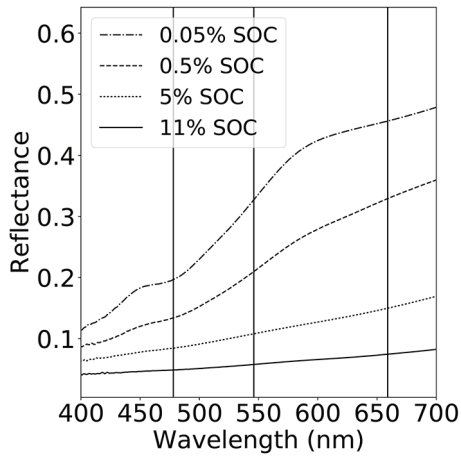

Fig. 7. Influence of soil organic C (SOC) on spectral reflectance. Examples of spectral curves for samples within the USDA Rapid Carbon Assessment database with SOC concentrations ranging from 0.05 to 11%. Vertical bars show the reflectance values used in the calculation of the SOC index: 478 nm (blue), 546 nm (green), and 659 nm (red).

REFERENCES

Adams, J.B., M.O. Smith, and P.E. Johnson. 1986. Spectral mixture modeling: A new analysis of rock and soil types at the Viking Lander 1 site. J. Geophys. Res. Solid Earth 91:8098–8112. doi:10.1029/JB091iB08p08098

Aldana-Jague, E., G. Heckrath, A. Macdonald, B. van Wesemael, and K. Van Oost. 2016. UAS-based soil carbon mapping using VIS-NIR (480–1000 nm) multi-spectral imaging: Potential and limitations. Geoderma 275:55–66. doi:10.1016/j.geoderma.2016.04.012

Bachofer, F., G. Quénéhervé, V. Hochschild, and M. Maerker. 2015. Multisensoral topsoil mapping in the semiarid Lake Manyara region, northern Tanzania. Remote Sens. 7:9563–9586. doi:10.3390/rs70809563

Baldridge, A., S. Hook, C. Grove, and G. Rivera. 2009. The ASTER spectral library version 2.0. Remote Sens. Environ. 113:711–715. doi:10.1016/j.rse.2008.11.007

Bartholomeus, H., M. Schaepman, L. Kooistra, A. Stevens, W. Hoogmoed, and O. Spaargaren. 2008. Spectral reflectance based indices for soil organic carbon quantification. Geoderma 145:28–36. doi:10.1016/j.geoderma.2008.01.010

Ben-Dor, E., and A. Banin. 1995. Near-infrared analysis as a rapid method to simultaneously evaluate several soil properties. Soil Sci. Soc. Am. J. 59:364–372. doi:10.2136/sssaj1995.03615995005900020014x

Cambardella, C., T. Moorman, T. Parkin, D. Karlen, J. Novak, R. Turco, and A. Konopka. 1994. Field-scale variability of soil properties in central Iowa soils. Soil Sci. Soc. Am. J. 58:1501–1511. doi:10.2136/sssaj1994.03615995005800050033x

Chang, C., D.A. Laird, M.J. Mausbach, and C.R. Hurburgh. 2001. Near-infrared reflectance spectroscopy–principal components regression analyses of soil properties. Soil Sci. Soc. Am. J. 65:480–490. doi:10.2136/sssaj2001.652480x

Chen, F., D.E. Kissel, L.T. West, and W. Adkins. 2000. Field-scale mapping of surface soil organic carbon using remotely sensed imagery. Soil Sci. Soc. Am. J. 64:746–753. doi:10.2136/sssaj2000.642746x

Chikhaoui, M., F. Bonn, A.I. Bokoye, and A. Merzouk. 2005. A spectral index for land degradation mapping using ASTER data: Application to a semi-arid mediterranean catchment. Int. J. Appl. Earth Obs. Geoinf. 7:140–153. doi:10.1016/j.jag.2005.01.002

Dogan, H.M., and O.M. Kılıç. 2013. Modelling and mapping some soil surface properties of Central Kelkit Basin in Turkey by using Landsat-7 ETM images. Int. J. Remote Sens. 34:5623–5640. doi:10.1080/01431161.2013.796097

Escadafal, R. 1993. Remote sensing of soil color: Principles and applications. Remote Sens. Rev. 7:261–279. doi:10.1080/02757259309532181

Frazier, B., and Y. Cheng. 1989. Remote sensing of soils in the eastern Palouse region with Landsat Mhematic mapper. Remote Sens. Environ. 28:317–325. doi:10.1016/0034-4257(89)90123-5

Gomez, C., R.A.V. Rossel, and A.B. McBratney. 2008. Soil organic carbon prediction by hyperspectral remote sensing and field vis-NIR spectroscopy: An Australian case study. Geoderma 146:403–411. doi:10.1016/j.geoderma.2008.06.011

Huete, A., and R. Escadafal. 1991. Assessment of biophysical soil properties through spectral decomposition techniques. Remote Sens. Environ. 35:149–159. doi:10.1016/0034-4257(91)90008-T

Lal, R. 2004. Soil carbon sequestration impacts on global climate change and food security. Science 304:1623–1627. doi:10.1126/science.1097396

Lal, R. 2006. Enhancing crop yields in the developing countries through restoration of the soil organic carbon pool in agricultural lands. Land Degrad. Dev. 17:197–209. doi:10.1002/ldr.696

Li, D., X. Chen, Z. Peng, S. Chen, W. Chen, L. Han, and Y. Li. 2012. Prediction of soil organic matter content in a litchi orchard of south China using spectral indices. Soil Tillage Res. 123:78–86. doi:10.1016/j.still.2012.03.013

Li, X., G.W. McCarty, D.L. Karlen, and C.A. Cambardella. 2018. Topographic metric predictions of soil redistribution and organic carbon in Iowa cropland fields. Catena 160:222–232. doi:10.1016/j.catena.2017.09.026

Lilliefors, H.W. 1969. On the Kolmogorov-Smirnov test for the exponential distribution with mean unknown. J. Am. Stat. Assoc. 64:387–389. doi:10.1080/01621459.1969.10500983

McCarty, G.W., and J.B. Reeves. 2006. Comparison of near infrared and mid infrared diffuse reflectance spectroscopy for field-scale measurement of soil fertility parameters. Soil Sci. 171:94–102. doi:10.1097/01.ss.0000187377.84391.54

Mishra, U., R. Lal, B. Slater, F. Calhoun, D. Liu, and M. Van Meirvenne. 2009. Predicting soil organic carbon stock using profile depth distribution functions and ordinary kriging. Soil Sci. Soc. Am. J. 73:614–621. doi:10.2136/sssaj2007.0410

Mulder, V., S. De Bruin, M. Schaepman, and T. Mayr. 2011. The use of remote sensing in soil and terrain mapping: A review. Geoderma 162:1–19. doi:10.1016/j.geoderma.2010.12.018

Mulla, D.J. 2013. Twenty five years of remote sensing in precision agriculture: Key advances and remaining knowledge gaps. Biosyst. Eng. 114:358–371. doi:10.1016/j.biosystemseng.2012.08.009

Nanni, M.R., and J.A.M. Demattê. 2006. Spectral reflectance methodology in comparison to traditional soil analysis. Soil Sci. Soc. Am. J. 70:393–407. doi:10.2136/sssaj2003.0285

Nocita, M., A. Stevens, C. Noon, and B. van Wesemael. 2013. Prediction of soil organic carbon for different levels of soil moisture using vis-NIR spectroscopy. Geoderma 199:37–42. doi:10.1016/j.geoderma.2012.07.020

Omernik, J.M. 1987. Ecoregions of the conterminous United States. Ann. Assoc. Am. Geogr. 77:118–125. doi:10.1111/j.1467-8306.1987.tb00149.x

Palacios-Orueta, A., and S.L. Ustin. 1998. Remote sensing of soil properties in the Santa Monica Mountains I. Spectral analysis. Remote Sens. Environ. 65:170–183. doi:10.1016/S0034-4257(98)00024-8

Peón, J., C. Recondo, S.F. Fernández, J. Calleja, E. De Miguel, and L. Carretero. 2017. Prediction of topsoil organic carbon using airborne and satellite hyperspectral imagery. Remote Sens. 9:1211. doi:10.3390/rs9121211

Pimentel, D., C. Harvey, P. Resosudarmo, K. Sinclair, D. Kurz, M. McNair, S. Crist, L. Shpritz, L. Fitton, and R. Saffouri. 1995. Environmental and economic costs of soil erosion and conservation benefits. Science 267:1117–1122. doi:10.1126/science.267.5201.1117

Reeves, D. 1997. The role of soil organic matter in maintaining soil quality in continuous cropping systems. Soil Tillage Res. 43:131–167. doi:10.1016/S0167-1987(97)00038-X

Rossel, R.V., and T. Behrens. 2010. Using data mining to model and interpret soil diffuse reflectance spectra. Geoderma 158:46–54. doi:10.1016/j.geoderma.2009.12.025

Rossel, R.V., D. Walvoort, A. McBratney, L.J. Janik, and J. Skjemstad. 2006. Visible, near infrared, mid infrared or combined diffuse reflectance spectroscopy for simultaneous assessment of various soil properties. Geoderma 131:59–75. doi:10.1016/j.geoderma.2005.03.007

Roy, D.P., M. Wulder, T.R. Loveland, C. Woodcock, R. Allen, M. Anderson, D. Helder, J. Irons, D. Johnson, and R. Kennedy. 2014. Landsat-8: Science and product vision for terrestrial global change research. Remote Sens. Environ. 145:154–172. doi:10.1016/j.rse.2014.02.001

Schulze, D.G., J.L. Nagel, G.E. Van Scoyoc, T.L. Henderson, M.F. Baumgardner, and D.E. Stott. 1993. Significance of organic matter in determining soil colors. In: J.M. Bigham and E.J. Ciolkosz, editors, Soil color. SSSA Spec. Publ. 31. SSSA, Madison, WI. p. 71–90. doi:10.2136/sssaspecpub31.c5

Sequeira, C.H., S.A. Wills, S. Grunwald, R.R. Ferguson, E.C. Benham, and L.T. West. 2014. Development and update process of VNIR-based models built to predict soil organic carbon. Soil Sci. Soc. Am. J. 78:903–913. doi:10.2136/sssaj2013.08.0354

Smith, G.M., and E.J. Milton. 1999. The use of the empirical line method to calibrate remotely sensed data to reflectance. Int. J. Remote Sens. 20:2653–2662. doi:10.1080/014311699211994

Soil Survey Staff. 2013. Rapid Carbon Assessment (RaCA) project. USDA–NRCS. https://data.nal.usda.gov/dataset/rapid-carbon-assessment-raca (accessed 21 Feb. 2018).

Stevens, A., T. Udelhoven, A. Denis, B. Tychon, R. Lioy, L. Hoffmann, and B. Van Wesemael. 2010. Measuring soil organic carbon in croplands at regional scale using airborne imaging spectroscopy. Geoderma 158:32–45. doi:10.1016/j.geoderma.2009.11.032

Stoner, E.R., and M. Baumgardner. 1981. Characteristic variations in reflectance of surface soils. Soil Sci. Soc. Am. J. 45:1161–1165. doi:10.2136/sssaj1981.03615995004500060031x

Weidong, L., F. Baret, G. Xingfa, T. Qingxi, Z. Lanfen, and Z. Bing. 2002. Relating soil surface moisture to reflectance. Remote Sens. Environ. 81:238–246. doi:10.1016/S0034-4257(01)00347-9

West, T.O., and W.M. Post. 2002. Soil organic carbon sequestration rates by tillage and crop rotation. Soil Sci. Soc. Am. J. 66:1930–1946. doi:10.2136/sssaj2002.1930

Wijewardane, N.K., Y. Ge, S. Wills, and T. Loecke. 2016. Prediction of soil carbon in the conterminous United States: Visible and near infrared reflectance spectroscopy analysis of the rapid carbon assessment project. Soil Sci. Soc. Am. J. 80:973–982. doi:10.2136/sssaj2016.02.0052

Wills, S., T. Loecke, C. Sequeira, G. Teachman, S. Grunwald, and L.T. West. 2014. Overview of the U.S. Rapid Carbon Assessment Project: Sampling design, initial summary and uncertainty estimates. In: A. Hartemink and K. McSweeney, editors, Soil carbon: Progress in soil science. Springer, Cham, Switzerland. p. 95–104. doi:10.1007/978-3-319-04084-4_10